The effect of collisional quenching of the O 3p 3 P J state on the determination of the spatial distribution of the atomic oxygen density in an APPJ operating in ambient air by TALIF

The effect of collisional quenching of the O 3p ^3P_J state on the determination of the spatial distribution of the atomic oxygen density in an APPJ operating in ambient air by TALIF

2014 Plasma Sources Sci. Technol. 23 025012

(http://iopscience.iop.org/0963-0252/23/2/025012)

IOP Publishing Plasma Sources Science and Technology

Plasma Sources Sci. Technol. **23** (2014) 025012 (8pp) doi:10.1088/0963-0252/23/2/025012

The effect of collisional quenching of the O 3p ^3P_J state on the determination of the spatial distribution of the atomic oxygen density in an APPJ operating in ambient air by TALIF

S Zhang[1], A F H van Gessel[1], S C van Grootel[1] and P J Bruggeman[1,2]

[1] Eindhoven University of Technology, Department of Applied Physics, PO Box 513, 5600 MB, Eindhoven, The Netherlands
[2] University of Minnesota, Department of Mechanical Engineering, 111 Church Street SE, Minneapolis, MN 55455, USA

Received 30 August 2013, revised 29 January 2014
Accepted for publication 30 January 2014
Published 20 March 2014

Abstract

The spatial profile of the absolute atomic oxygen density is obtained by two-photon absorption laser-induced fluorescence (TALIF) in an Ar+2% air cold atmospheric pressure plasma jet (APPJ) operating in ambient air. The varying air concentration in the jet effluent which contributes to the collisional quenching of the O 3p ^3P_J state, pumped by the laser, strongly influences the recorded TALIF signal under the present experimental conditions. The spatially resolved air densities obtained from Raman scattering measurements have been reported in our previous work (van Gessel *et al* 2013 *Appl. Phys. Lett.* **103** 064103). These densities allow us to calculate the spatially dependent collisional quenching rate for the O 3p ^3P_J state and reconstruct the spatial O density profile from the recorded TALIF signal. Significant differences between the TALIF intensity profile and the actual O density profile for the investigated experimental conditions are found.

Keywords: collisional quenching, atomic density, TALIF

(Some figures may appear in colour only in the online journal)

1. Introduction

Cold atmospheric pressure plasma jets (APPJs) have attracted considerable interest because of their potential biomedical applications and surface treatment of heat-sensitive materials [2–4]. The effluent, which includes many reactive species, enables plasma jets to inactivate bacteria and contribute to wound healing [5]. One of the important species produced in APPJs is atomic oxygen. It is the precursor to the long-lived ozone which is bactericidal. In addition, atomic oxygen is believed to be important for material treatment [6]. As the effluent, including the atomic oxygen species, is blown towards the substrate, one requires the radial and axial distribution of atomic oxygen together with the gas velocity flow pattern to obtain the total flux which is important for the applications. In this work we only focus on the density of atomic oxygen.

Two-photon absorption laser-induced fluorescence (TALIF) is a widely used laser diagnostic method to obtain the atomic oxygen density [7–13]. TALIF is also used in this work. The ground state of atomic oxygen $2p^4\ ^3P_J$ is excited by two photons of 225.59 nm to the level $3p\ ^3P_J$. The excited O de-excites to the lower state $3s\ ^3S$ by emitting a photon at 844.58 nm. The amount of fluorescence at 844.58 nm allows one to deduce the absolute O density in the ground state when a proper calibration is made. Absolute calibration methods for O TALIF measurements by TALIF on xenon are well established (see, e.g., [7]).

The above description is, however, strongly complicated at atmospheric pressure due to significant collisional quenching of the excited state. In He–air mixtures in a MW jet, as shown in our previous work [14], the effective lifetime of the excited state of O could be measured even when using a nanosecond pulsed laser and the effect of quenching was determined from the TALIF measurements themselves. As we will show, the effective lifetime of the laser-excited O is very short under the present experimental conditions to measure the fluorescence decay when using a nanosecond pulsed laser. Hence the quenching rate needs to be calculated and the densities of the quenchers need to be known or determined. In addition, the air diffusion into the jet effluent causes a spatial dependence of the collisional quenching which requires the knowledge of the spatial variation in the density of the quenchers.

Duluard *et al* used mass spectrometry and LIF on OH radicals to estimate the intrusion of air in an Ar/O_2 RF atmospheric pressure plasma [15]. Yonemori *et al* obtained the 2D distribution of air–helium mixture ratio in a helium atmospheric plasma jet by LIF on OH radical which has a longer effective lifetime compared with the O 3p ^3P_J state [16]. Reuter *et al* used VUV absorption to measure the air concentration in an argon plasma jet but only obtained and reported the effect of quenching on the determination of the O density on the axis of symmetry. The effect of quenching was reported to be negligible [11]. In fact this result is to be expected, since the maximum reported air concentration on the axial position between 0 and 7 mm from the nozzle is less than 5% in [11]. However, the air density gradient is significantly larger in the radial direction so collisional quenching effects are important in this case, as will be shown in this work.

After a description of the experimental setup and conditions, the time and spatially resolved TALIF intensities are reported. Next the air concentrations and gas temperature 2D profiles used to correct for the collisional quenching are shown. Finally, we present the absolutely calibrated 2D atomic oxygen densities in the jet effluent corrected for spatially varying quenching rates. The accuracy of this correction is also discussed.

2. Experimental setup and conditions

The APPJ, which is identical to the one used in previous work [1, 17–19], is driven by 13.56 MHz RF modulated by 20 kHz waveform with the duty ratio 20% (10 μs on, 40 μs off). The feeding gas is 1 slm argon mixed with 2% air. The obtained average power dissipated by the plasma is 3.5 W. Details about the plasma jet and the power measurement can be found in [17, 20]. The TALIF measurement is implemented identical as in our previous reported work [14]. The schematic representation of the TALIF measurement is shown in figure 1. The wavelength of 225.5 nm, necessary for the TALIF measurement, is produced by a dye laser (Sirah, CSTR-LG-3000-HRR) which is pumped by the third harmonic of a Nd : YAG laser (Edgewave, IS6III-E YAG). The 1 kHz laser system is synchronized with the RF signal applied to the plasma and the detecting unit by a delay generator (BNC, Model 575 pulse/delay generator). The UV laser

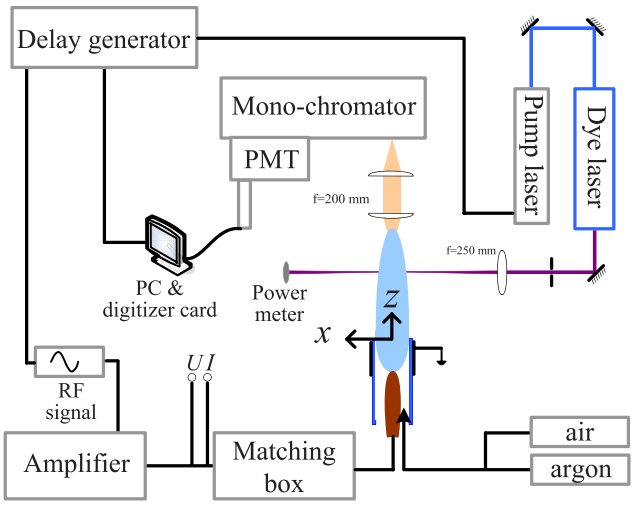

Figure 1. Schematic representation of the TALIF setup.

beam is focused into the plasma effluent by a convex lens ($f = 250$ mm). The fluorescence light (844.68 nm for atomic oxygen) is collected perpendicularly to the laser beam axis and imaged by two lenses ($f = 200$ mm) onto the 100 μm entrance slit of a monochromator (Jarrell-Ash 82025, 0.5 m focal length, 1180 grooves mm^{-1} grating). A photomultiplier (Hamamatsu R666), used as a detector on the monochromator, operates in the photon counting mode. The counting mode is achieved by a Fast Comtec P7888 time digitizer card with a time resolution of 1 ns. A laser energy meter (Ophir PD10) is used to obtain the laser energy of every pulse. The used laser system and absolute calibration method for TALIF, based on the measurement of the fluorescence light of state $6p'[3/2]_2 \rightarrow 6s'[1/2]_1$ of a known Xe concentration in all He–Xe mixture, are described in more detail in [14].

It should be noted that in this work the measurements of TALIF are performed by scanning the laser wavelength around 225.59 nm and fixing the wavelength of the monochromator at 884.68 nm. The ground state (O $2p^4\ ^3P_J$) and upper state (O $3p\ ^3P_{J'}$) consist of three levels with orbital angular momentum quantum numbers 2, 1, 0. The upper levels are spaced closer than the laser bandwidth and cannot be distinguished during laser excitation and fluorescence detection. The lower levels have an energy spacing much larger than the laser bandwidth, and are individually excited. As is shown in figure 2, the laser is scanned around the transition corresponding to the $J = 2$ level of the ground state and the total fluorescence integrated over the line profile is used as the fluorescence intensity for the absolute measurements. The total ground state O density is obtained by assuming a Boltzmann distribution of the three J-levels in the ground state with a temperature equal to the gas temperature. This approach has been validated in our previous work [14].

A high laser intensity is critical for TALIF measurements. As a consequence, saturation and other effects correlated with the large intensity such as three-photon ionization and photo-dissociation can occur. To assess this effect both the beam waist and the TALIF intensity as a function of the laser energy have been recorded.

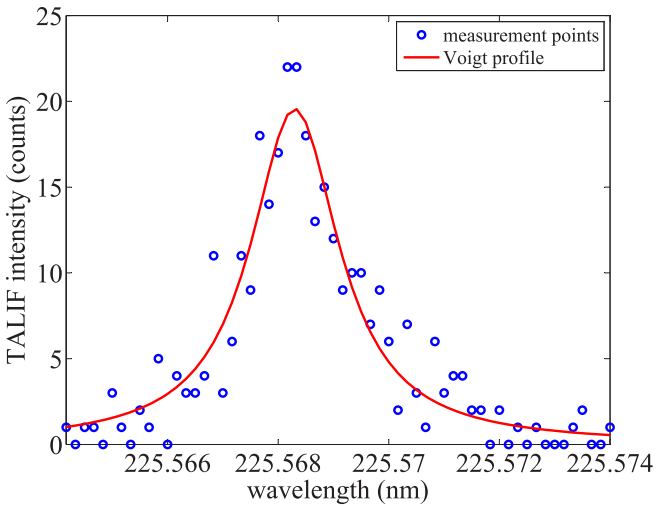

Figure 2. TALIF intensity obtained by scanning the laser through the O 3p $^3P_2 \rightarrow$ 3p $^3P_{J'}$ transition. The measurement position is $z = 1$ mm and $r = 0$ mm. The laser energy is 5 μJ.

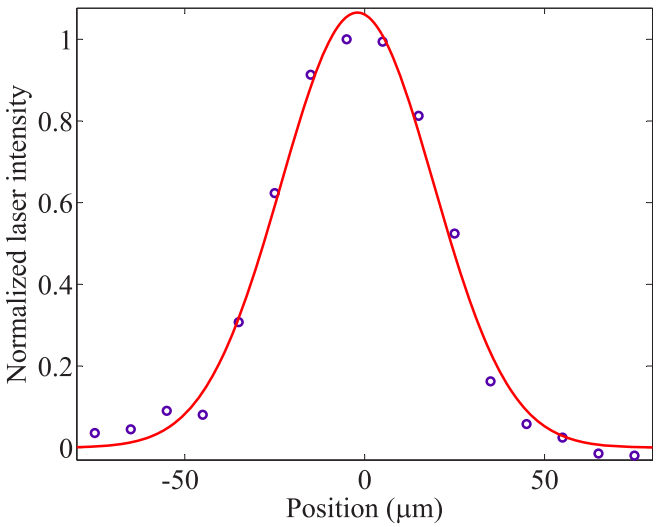

Figure 3. The beam waist of the laser at the TALIF measurement position in the z-direction, measured as indicated in the text. The profile is fitted with a Gaussian function and the FWHM is 42 μm.

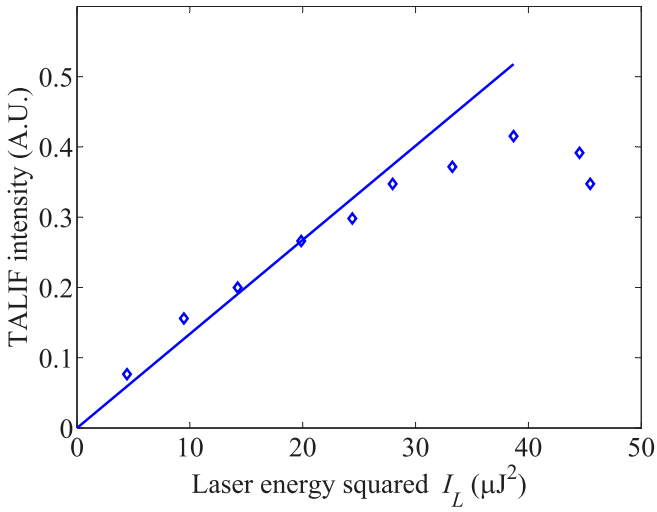

Figure 4. Recorded TALIF intensity as a function of the laser energy squared. The measurement position is chosen at $z = 1$ mm and $r = 0$ mm. The beam waist is 42 μm.

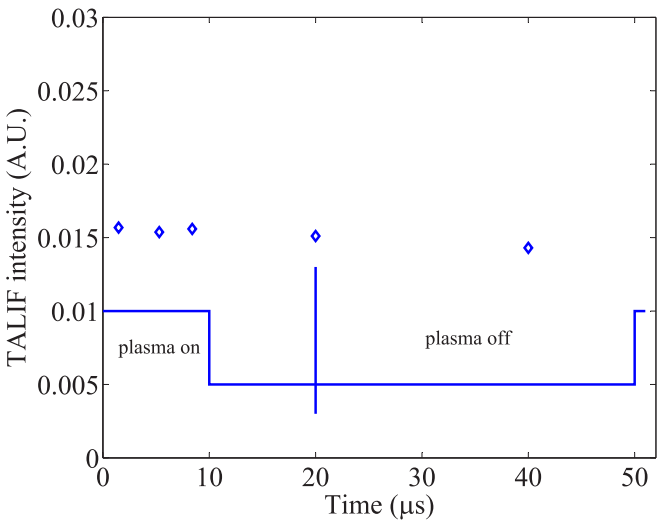

Figure 5. Time-resolved TALIF signal during one modulation period of the plasma. The TALIF signal is recorded at $z = 1$ mm and $r = 0$ mm.

The beam waist is obtained by recording the laser intensity when a sharp knife edge is moved in steps of 10 μm through the beam. The recorded laser intensity (I_L) yields the integral of the two-dimensional laser profile up to the position of the knife edge. Assuming that the laser intensity can be written as $I(x, y) = f(x) \times g(y)$, the derivative of the measured value yields the intensity distribution in the direction the knife edge was moved. The deduced full-width at half-maximum (FWHM) of the beam waist is 42 μm (figure 3).

The TALIF signal as function of I_L is shown in figure 4. It shows that for laser energies lower or equal to 5 μJ, the TALIF signal is proportional to I_L^2. In this work, all the TALIF measurements are performed under the conditions that the laser energy is between 4 and 5 μJ. It is noted that in our previous work [14] a higher energy of the 'linear regime' has been found for He plasmas using the same optics.

As there are some fluctuations in the power measurements presented in figure 4, we provide some additional information to estimate the validity of the TALIF measurements. The depletion of the ground state is negligible as an estimation of the ratio of the population on upper and lower states leads to 7×10^{-3}. The detection limit of TALIF in this work is 10^{19} m^{-3} and in the far effluent, where the O_2 density is the highest, no TALIF signal is observed. This means that photo-dissociation can be neglected in the present experiment. In addition, also the dominant depopulation mechanism of the excited state of O needs to be larger than the depopulation by photo-ionization of the state. With a peak laser intensity of 60 MW cm^{-2}, the photo-ionization rate is 3.6×10^7 Hz [21]. Although the photo-ionization rate is close to the spontaneous emission rate of the excited state (2.9×10^7 Hz), it remains much lower than the effective depopulation rate ($\sim 10^9$ Hz or smaller). Photo-ionization can thus also safely be neglected in the present experiment.

The spatial resolution of the TALIF measurement in the z-direction corresponds to the beam waist while the radial

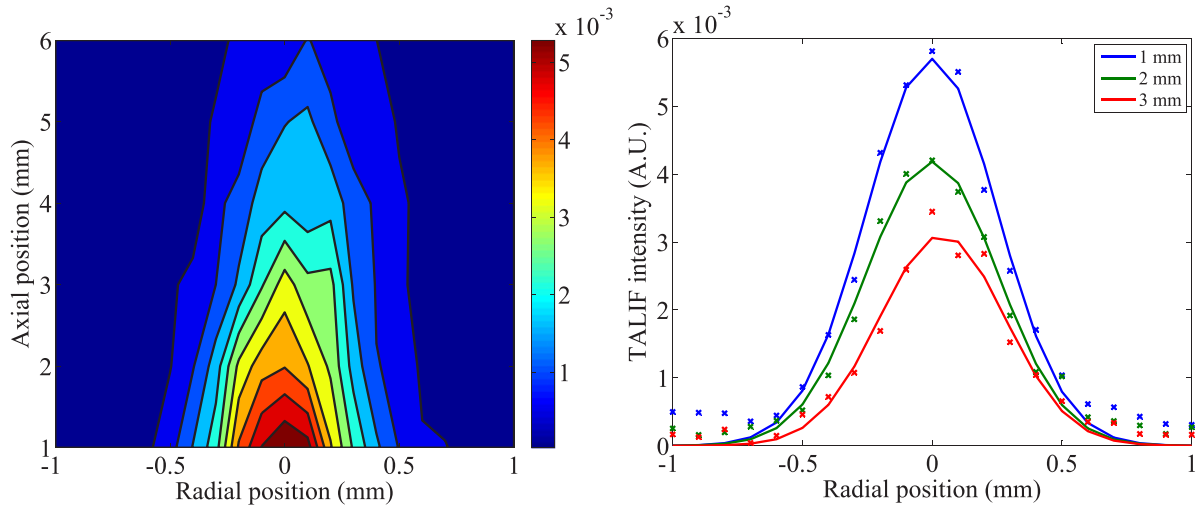

(a) TALIF intensity (A.U.) (b)

Figure 6. (*a*) The 2D profile of the recorded TALIF signal of atomic oxygen. (*b*) The radial distribution of the TALIF signal at $z = 1$, 2 and 3 mm. The original data (crosses) are fitted to a Gaussian profile. The position (0,0) corresponds to the position at the nozzle on the axis of symmetry of the jet.

resolution is in good approximation equal to the entrance slit of the spectrometer which is 100 μm.

3. Results and discussions

3.1. Time and spatially resolved TALIF signal

The RF plasma is power modulated at 20 kHz with a duty cycle of 20%. Figure 5 shows the corresponding TALIF signal as a function of time during the plasma on and off at a fixed position. It can be concluded from this figure that the TALIF signal is, to a good approximation, constant during one period. Also the gas temperature has been found equal in the plasma on and off case [18]. All the measurements in this work are carried out 10 μs after the plasma is switched off. This is done to avoid a strong time modulated background of the plasma emission (during the RF cycle) which reduces the signal-to-noise ratio of the recorded TALIF signal.

The recorded 2D TALIF intensities are shown in figure 6. The signal has been recorded in steps of 100 μm in the radial direction and 1 mm in the axial direction. For every axial position, a Gaussian function is used to fit the radial profile, as show in figure 6(*b*).

3.2. Gas temperature and air concentration profiles

As mentioned above, the gas temperature is used to obtain the total ground state oxygen atom density from the measurement of one level of the triplet state. In addition, the collisional quenching rate is dependent on the gas temperature and the species densities. The air densities are obtained directly but the Ar densities are calculated considering the local gas temperatures. The gas temperature distribution is taken from [18] and was obtained by Rayleigh scattering for identical plasma conditions. The 2D temperature profile and radial profiles for three axial positions are shown in figure 7.

The diffusion of ambient air into the plasma effluent has a large effect on the effluent chemistry. In addition, as mentioned above, it decreases the TALIF signal by collisional quenching with the excited level of atomic oxygen (3p ^3P_J) as the coefficients for collisional quenching by O_2 and N_2 are larger than for Ar (see next section). To obtain the collisional quenching from the ambient species, spatial-resolved air densities are needed. In this work the Raman scattering data from our previous publication [1], which reported 2D profiles of the air density, as shown in figure 8, are used. The air densities are expected to have a similar accuracy as the quenching rates, considering that the vibrational temperature of the ground state is not exceeding 1500 K and the metastable densities of N_2 and O_2 are not excessively large.

3.3. Collisional quenching of the 3p ^3P_J *state*

The obtained TALIF intensity is proportional to the branching ratio of the 3p ^3P_J state of O:

$$a = \frac{A_{23}}{A_2 + Q} \tag{1}$$

in which, A_{23} is the radiative decay rate of the energy level 3p $^3P_J \rightarrow$ 3s ^3S; A_2 is the total radiative decay rate of 3p ^3P_J to other energy level; Q is the collisional quenching rate of 3p ^3P_J. A_{23} and A_2 are both 2.88×10^7 s^{-1} [7, 14].

Ideally, the collisional quenching should be measured by the fluorescence decay. An example of the time-resolved fluorescence intensity on the position with the smallest air concentration (and thus lowest quenching rate, $z = 1$ mm and $r = 0$ mm) is shown in figure 9. The laser pulse is measured from recording the Rayleigh scattering intensity. The fluorescence signal is fitted with a convolution of the laser intensity squared with an exponential decay. The decay time corresponds to 1.25 ± 0.75 ns. This corresponds to a quenching rate of (0.5–2) $\times 10^{-9}$ s^{-1}. The large error on this value does

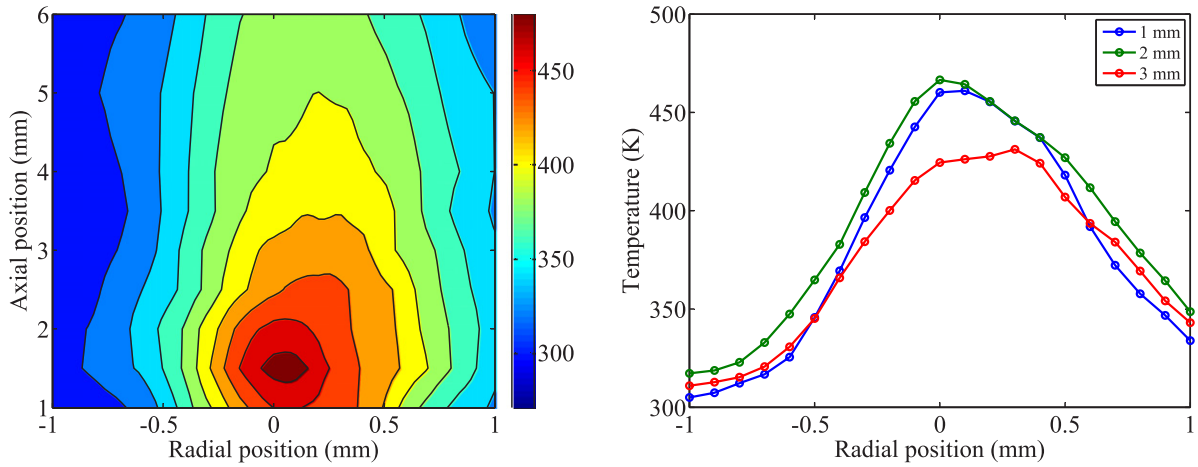

Figure 7. (*a*) 2D profile of the gas temperature and (*b*) the radial distribution of the gas temperature at $z = 1$, 2 and 3 mm [18].

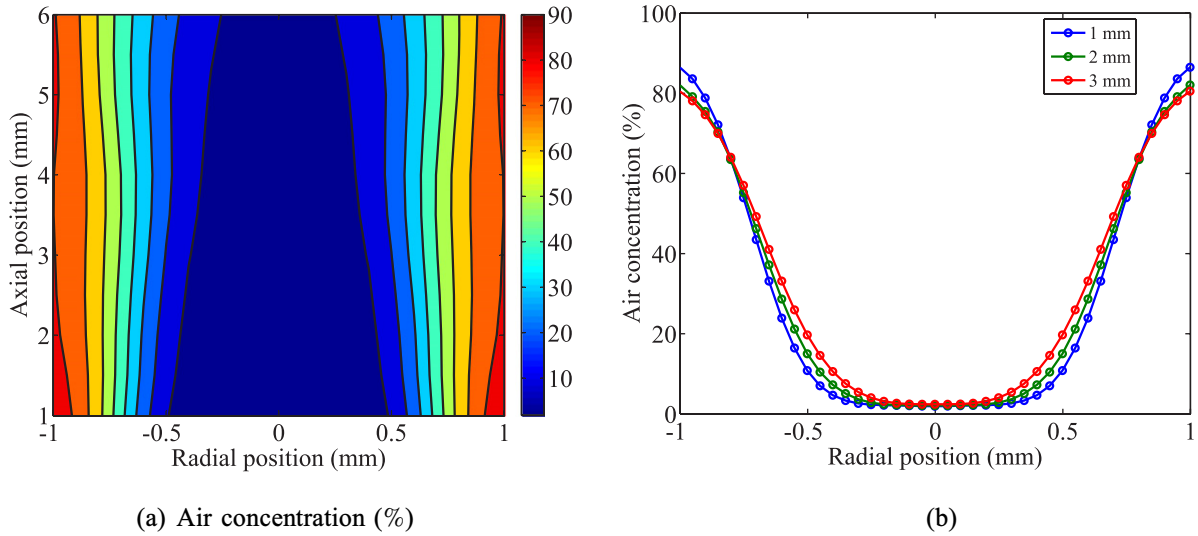

Figure 8. (*a*) 2D profile of the air concentration and (*b*) the radial distribution of the air concentration at $z = 1$, 2 and 3 mm [1].

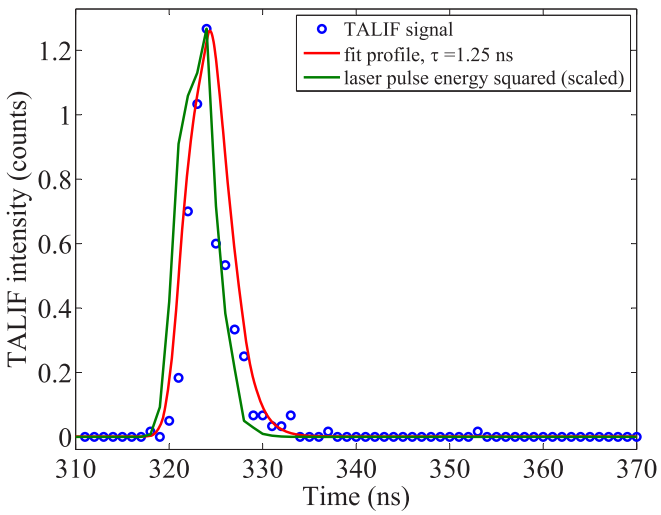

Figure 9. Time-resolved TALIF signal during one modulation period of the plasma.

not allow us to obtain accurate densities and a calculation of the quenching rate is necessary.

The collisional quenching rate coefficients used in this work are shown in table 1. However, it should be noted that the collisional quenching rate coefficient varies with the temperature. To the authors' knowledge no experimentally obtained temperature dependences of quenching rate coefficients are published for the considered excited state of atomic oxygen and it is therefore assumed that the quenching rate coefficient has the following temperature dependence [23, 24]:

$$k_q = \sigma_q \langle v \rangle \propto T^{-1/2} \tag{2}$$

with $\langle v \rangle$ the average thermal velocity which is proportional to the inverse root of the gas temperature. In fact, theoretical work shows that the cross section (σ_q) has a modest temperature dependence [25].

For the current experimental conditions, the collisional quenching is mainly due to the ambient species from diffused

Table 1. Collisional quenching rates used in this work at 300 K.

Species	Quenching rate coefficient (10^{-16} m^3 s^{-1})	Max. conc. (m^{-3})	Max. quenching rate (s^{-1})	
N_2	5.9 ± 0.2	1.72×10^{24}[a]	1.01×10^{10}	[22]
O_2	9.4 ± 0.5	4.0×10^{25}[a]	3.76×10^{9}	[7]
Ar	0.14 ± 0.007	1.85×10^{25}[a]	2.58×10^{8}	[7]
H_2O	49 ± 3	~1.8% of n_{air}[b]	1.87×10^{9}	[13]

[a] Estimated from the data presented in figures 7 and 8.
[b] The relative humidity in the lab is assumed not to exceed 80%.

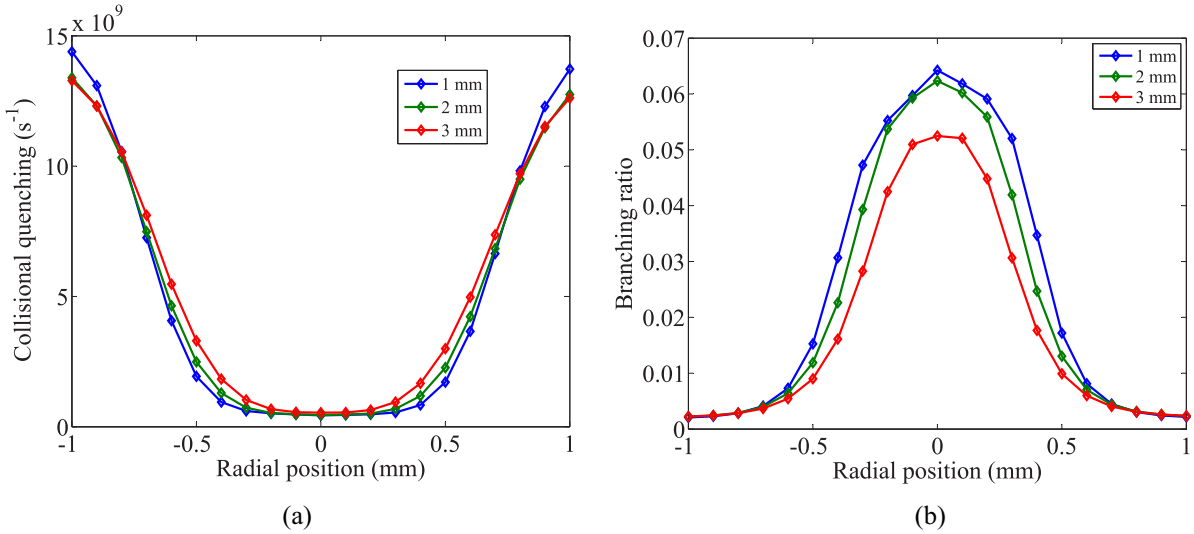

Figure 10. The calculated radial distribution of (*a*) collisional quenching rate and (*b*) branching ratio at $z = 1$, 2 and 3 mm.

(humid) air and Ar. This can also be verified from table 1. As a result, Q in this work is obtained as follows:

$$Q = k_{O_2} n_{O_2} + k_{Ar} n_{Ar} + k_{N_2} n_{N_2}. \quad (3)$$

The radial dependence of the collisional quenching rate and branching ratio for three different axial positions is shown in figure 10. It can be seen that the collisional quenching depends significantly on the air concentration in the plasma effluent.

In the rest of this section, the accuracy of the calculated quenching rates will be evaluated.

The effect of humidity with a realistic upper estimate of a relative humidity of 80% corresponding to 1.8% water in the lab air, could lead to a 13% underestimate of the effect of the quenching introduced by the humid air which is entering the jet effluent by diffusion. This underestimate is considered to be acceptable in this work as it is similar to the error on the O density induced by the accuracy of the reported quenching rates.

The plasma also changes the gas composition *in situ*. The main difference in species in the core of the plasma would be caused by the dissociation of O_2, forming O. However, we measured the O_2 density by Raman and the O density is not expected to exceed 18.5% of the O_2 density. As the quenching rate for O is smaller than 0.2 times the quenching rate for O_2 [12] the O_2 dissociation process is not significantly influencing the calculated overall quenching rate. It should be noted that the density of other species or radicals produced by the plasma, such as NO or O_3, is not expected to exceed 10^{21} m^{-3} [17, 18]. This is two orders smaller than the air density in the core of the effluent and is thus not expected to influence the quenching rates.

Three-body quenching processes can play a role at elevated pressures. In our previous work, indeed three-body quenching in Xe TALIF was observed starting at 400 mbar [14]. To the authors' knowledge, a similar effect is not reported for O. The accuracy of the measured decay time is too small to enable us to check the potential effect of three-body quenching. In the literature, O quenching by Ar has been measured up to 0.1 bar by Bittner *et al* [26], who showed a linear dependence with pressure. Several other groups have also used extrapolated quenching coefficients [7].

3.4. O density

The atomic oxygen density, absolutely calibrated and corrected for spatial-dependent quenching, is shown in figure 11. Taking into consideration the collisional quenching due to the air diffusion, the radial density profile of atomic oxygen becomes broader. Within a cylinder with radius 0.3 mm (at least close to the nozzle), the air concentration is lower than 5%, and the atomic oxygen density profile is almost identical to the TALIF signal profile. This is consistent with the findings of Reuter *et al* [11]. Outside this cylinder of 0.3 mm, the air concentration starts to increase with a steep gradient between

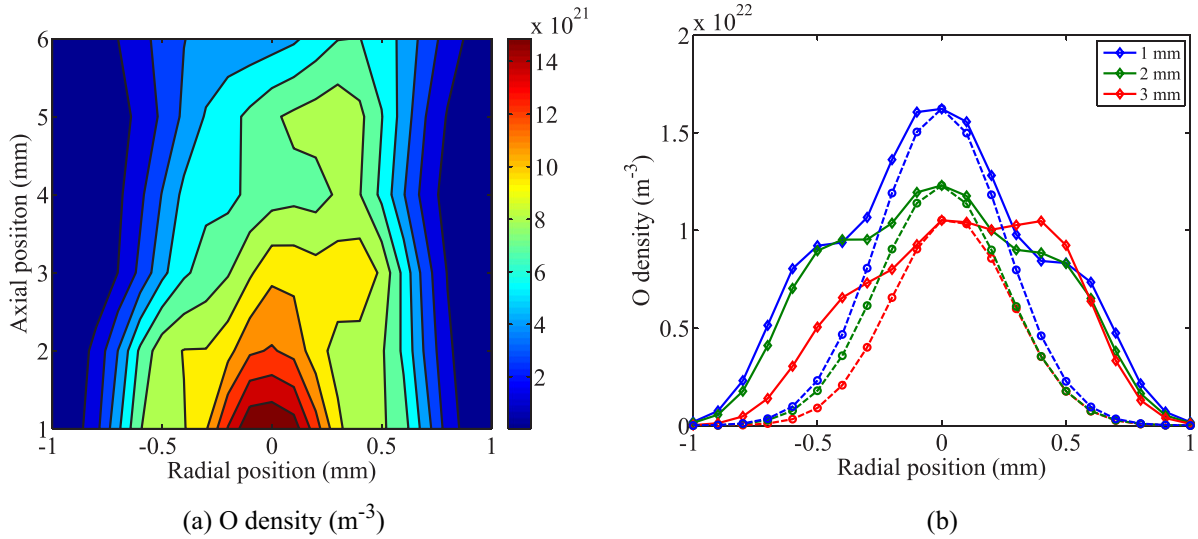

(a) O density (m^{-3}) (b)

Figure 11. (*a*) The obtained 2D distribution of the O density, (*b*) O density profile at $z = 1, 2, 3$ mm. The dashed line which corresponds to the normalized TALIF signal is given as a reference.

0.3 and 0.6 mm. At this position, collisional quenching significantly starts to reduce the fluorescence intensity and needs to be taken into account.

For an identical plasma jet a depletion of the ozone is found in the core of the jet effluent and the maximum of the O_3 density is located at a radial distance of 0.9 mm [17]. This would not be expected if the O density was the same as the recorded TALIF profile, but is consistent with the O density profile shown in figure 11(*a*). In fact, with the corrected profiles, the O_3 density starts to increase at the same position where the O density reduces with a steep gradient. This is necessary as, despite the fact that a significant density of O is necessary to produce ozone, a very large density of O will destroy it by the reaction $O + O_3 \rightarrow 2O_2$ [17].

A similar important effect of quenching on the determination of the O density is found at axial distances in excess of 3 mm. This distance is smaller than what has been found in a similar jet by Reuter *et al*. It might be explained by the fact that there is more air diffusion in the jet reported in this work due to the higher flow rate of argon used in the cited work (1 slm compared with 5 slm). The flow pattern is expected to be different from the present case. However, as can be seen from figure 11(*a*), the O density reduces and the air density increases for the zone where $z > 3$ mm which decreases the accuracy of the TALIF measurements. It is thus important to consider spatially resolved quenching for each jet individually as it strongly depends on the flow pattern which can be influenced by the gas temperature, discharge morphology, exact jet geometry and flow rates.

4. Conclusion

It is shown that spatially dependent collisional quenching due to air density gradients in an Ar RF APPJ operating open to air needs to be considered to determine the spatially resolved O density profile from TALIF measurements. The radial O density profiles are significantly broader than the recorded TALIF signal. These broader density profiles are found to be consistent with the O_3 depletion zone diameter found in the core of the jet for which the ozone depletion is ascribed to quenching of ozone by atomic oxygen.

Acknowledgments

This work is partially funded by the Dutch Technology Foundation (STW). The authors sincerely thank Eddie van Veldhuizen, Huib Schouten, Ab Schrader and Evert Ridderhof for their technical assistance with experiments.

References

[1] van Gessel B, Brandenburg R and Bruggeman P 2013 *Appl. Phys. Lett.* **103** 064103
[2] Kong M G, Kroesen G, Morfill G, Nosenko T, Shimizu T, van Dijk J and Zimmermann J L 2009 *New J. Phys.* **11** 115012
[3] Schutze A, Jeong J Y, Babayan S E, Park J, Selwyn G S and Hicks R F 1998 *IEEE Trans. Plasma Sci.* **26** 1685–94
[4] Samukawa S *et al* 2012 *J. Phys. D: Appl. Phys.* **45** 253001
[5] Laroussi M 2009 *IEEE Trans. Plasma Sci.* **37** 714–25
[6] Reuter R, Rügner K, Ellerweg D, de los Arcos T, von Keudell A and Benedikt J 2012 *Plasma Process. Polym.* **9** 1116–24
[7] Niemi K, Schulz-von der Gathen V and Döbele H 2005 *Plasma Sources Sci. Technol.* **14** 375
[8] Oda T, Yamashita Y, Takezawa K and Ono R 2006 *Thin Solid Films* **506** 669–73
[9] Reuter S, Niemi K, Schulz-von der Gathen V and Döbele H F 2008 *Plasma Sources Sci. Technol.* **18** 015006
[10] Stancu G D, Kaddouri F, Lacoste D and Laux C 2010 *J. Phys. D: Appl. Phys.* **43** 124002
[11] Reuter S, Winter J, Schmidt-Bleker A, Schroeder D, Lange H, Knake N, Schulz-von der Gathen V and Weltmann K D 2012 *Plasma Sources Sci. Technol.* **21** 024005
[12] Dilecce G, Vigliotti M and De Benedictis S 2000 *J. Phys. D: Appl. Phys.* **33** 53
[13] Meier U, Kohse-Höinghaus K and Just T 1986 *Chem. Phys. Lett.* **126** 567–73

[14] van Gessel A F H, Grootel S C and Bruggeman P J 2013 *Plasma Sources Sci. Technol.* **22** 055010
[15] Duluard C, Dufour T, Hubert J and Reniers F 2013 *J. Appl. Phys.* **113** 093303
[16] Yonemori S, Nakagawa Y, Ono R and Oda T 2012 *J. Phys. D: Appl. Phys.* **45** 225202
[17] Zhang S, van Gaens W, van Gessel B, Hofmann S, van Veldhuizen E, Bogaerts A and Bruggeman P 2013 *J. Phys. D: Appl. Phys.* **46** 205202
[18] van Gessel A, Alards K and Bruggeman P 2013 *J. Phys. D: Appl. Phys.* **46** 265202
[19] van Gils C, Hofmann S, Boekema B, Brandenburg R and Bruggeman P 2013 *J. Phys. D: Appl. Phys.* **46** 175203
[20] Hofmann S, van Gessel A F H, Verreycken T and Bruggeman P 2011 *Plasma Sources Sci. Technol.* **20** 065010
[21] Bamford D J, Jusinski L E and Bischel W K 1986 *Phys. Rev.* A **34** 185
[22] Uddi M, Jiang N, Mintusov E, Adamovich I V and Lempert W R 2009 *Proc. Combust. Inst.* **32** 929–36
[23] Frank J H and Settersten T B 2005 *Proc. Combust. Inst.* **30** 1527–34
[24] Ono R, Takezawa K and Oda T 2009 *J. Appl. Phys.* **106** 043302
[25] Faist M and Bernstein R 1976 *J. Chem. Phys.* **64** 3924
[26] Bittner J, Kohse-Höinghaus K, Meier U and Just T 1988 *Chem. Phys. Lett.* **143** 571–6